

## Separators with Active-Carbon Coating for Advanced Lithium–Sulfur Batteries

Yafang Guo<sup>1</sup>, Jianrong Xiao<sup>1,\*</sup>, Yongxuan Hou<sup>1</sup>, Yanwei Li<sup>2</sup>, Aihua Jiang<sup>1,\*</sup>

<sup>1</sup> College of science, Guilin University of Technology, Guilin 541004, PR China.

<sup>2</sup> Guangxi Key Laboratory of Electrochemical and Magneto-chemical Functional Materials, Guilin University of Technology, Guilin 541004, Guangxi, PR China

\*E-mail: [xjr@glut.edu.cn](mailto:xjr@glut.edu.cn), [jah@glut.edu.cn](mailto:jah@glut.edu.cn)

Received: 2 August 2017 / Accepted: 13 September 2017 / Published: 12 October 2017

---

Lithium–sulfur (Li–S) batteries have a large theoretical energy density and high theoretical capacity. However, practical applications of Li–S batteries are limited by cycling instability and low rate performance, which mainly originate from the intrinsic poor conductivity of sulfur and the dissolution of polysulfides generated during discharge–charge cycles. In this work, we demonstrate a low-cost, facile and effective strategy to modify separators with an active carbon layer. The carbon-coated separator can significantly increase the specific discharge capacity and improve cycling stability of the cathode prepared by the S powder and the active carbon. For example, the initial discharge capacity of the S cathode reaches up to 1452 mAh g<sup>-1</sup> at 0.2 C with a low fading rate of 0.15% per cycle within 400 cycles. Moreover, when the rate is increased to 1 C, the S cathode can still deliver a discharge capacity of 1009 mAh g<sup>-1</sup>. The enhanced electrochemical performance can be attributed to the excellent conductivity and strong adsorption capability of the active carbon coating, which effectively suppresses the shuttle effect of polysulfides. The electrochemical analysis confirmed the long cycle life, excellent rate performance, and high discharge capacity of the Li–S cells.

---

**Keywords:** separator; active carbon; polysulfide adsorption; lithium-sulfur battery

### 1. INTRODUCTION

Lithium–sulfur (Li–S) batteries are highly attractive for their high theoretical specific capacity of 1675 mAh g<sup>-1</sup> and energy density of 2600 Wh kg<sup>-1</sup>, which are much higher than lithium-ion battery[1-6] and can meet the ever-increasing demands for energy-storage applications, from electronic devices to electric vehicles[7,8]. In addition, sulfur has advantages of low cost, environmental benignity, and non-toxicity. However, the commercialization of Li–S batteries is still limited by

several drawbacks, such as electrical and ionic insulation of sulfur[9-11], volume expansion during conversion from sulfur to  $\text{Li}_2\text{S}$ [12,13], and shuttle effect of the polysulfides during the charge–discharge process[14]. As a result, Li–S batteries generally present a poor cycle life, low active material utilization, and rapidly declining capacity.

Tremendous efforts have been devoted to solve these problems, focusing mainly on modifying the S cathode. The strategies include immobilizing S in core–shell porous carbon spheres[15-20], fabricating conductive fibrous structures[21-23], and preparing 3D hierarchical polyporous composites[24,25]. Although these strategies can improve the loading of active mass due to the higher specific surface area and larger pore volume, the manufacturing processes are rather complicated, thereby limiting the commercialization of Li–S batteries. The modification of electrolytes[26,27] has also been explored to improve the rate capability and cycle life of Li–S batteries with distinguished achievements. Another promising solution is to insert an interlayer between the cathode and separator[28-33]. This strategy leads to lengthening cycle life and can effectively increase the electrochemical performance of Li–S batteries. However, the inter-layer cannot be made thin enough to guarantee a high energy density of Li–S cells.

The separator, which is as an indispensable component of Li–S batteries is usually made from polyethylene, polypropylene, or their composite. In Li–S cells, the separator is an electronic insulator but not ionic, which means the polysulfides ions can pass through without any obstacle. Accordingly, the inhibition of shuttle effect by modification the separator would be a convenient approach to improve the electrochemical properties of Li–S batteries. Lately, Super P[34-36], acetylene black[37], graphene[38,39], multi-walled carbon nanotubes[40-42], ketjen black[40,43], element doped carbon materials[44-47] and some metallic oxide[48-51] have been applied as an effective barrier layer between the cathode and separator, suppressing the shuttle effect by the physical and chemical absorption of the lithium(poly)sulfide intermediates. According to the previous findings of our research group, we know that active carbon (AC) has a multiporous structure and a superior adsorption capacity, which can effectively improve the electrochemical performance of Li–S cells when used as carbon matrix for cathode[52].

In this study, we report a simple and effective approach for reducing the influence of shuttle effect in lithium–sulfur batteries by employing a hybrid separator with a thin AC coating. With the AC-decorated separator, Li–S batteries exhibit a higher coulombic efficiency and an improved electrochemical performance with a high initial discharge capacity of  $1452 \text{ mAh g}^{-1}$  and maintain  $555 \text{ mAh g}^{-1}$  after 400 cycles at a discharge current of 0.2 C. These results demonstrate that the AC-coated separator has a more potential in applications of Li–S batteries.

## 2. EXPERIMENTAL SECTION

### 2.1. Preparation of AC-coated separator

First, commercial AC and polyvinylidene fluoride (PVDF) powder were mixed with mass ratio of 9:1, and then ground for 2 h. Subsequently the AC/PVDF mixture was placed in *N*-methyl-2-

pyrrolidinone solution (NMP) and went on grinding for half an hour to form homogeneous slurry. Finally, the slurry was coated on the cathode side of a pristine separator (Polypropylene, Celgard 2400), then dried in a vacuum oven at 60 °C for 12 h. Furthermore, the prepared sample was marked as AC-9, according to the mass ratios of AC/PVDF. In addition, the AC- $X$  ( $X = 7, 8$ ) composites were prepared similarly for comparison. A schematic illustration of the fabrication of the AC- $X$  separator is shown in Fig. 1a.

## 2.2. Preparation of AC/S active material

S and AC were placed in an agate mortar with a mass ratio of 7: 3 and ground for 1 h before transferring into a polytetrafluoroethylene reaction vessel. Then this reaction vessel was kept still and open in argon-filled glove box for 0.5 h to exclude the residual air so that S would not be oxidized at high temperature. Next, the reaction vessel was heated at 155 °C for 12 h. At this temperature, the melt sulfur can easily penetrate the pores of AC. After cooling down to room temperature, the AC/S composite was obtained.

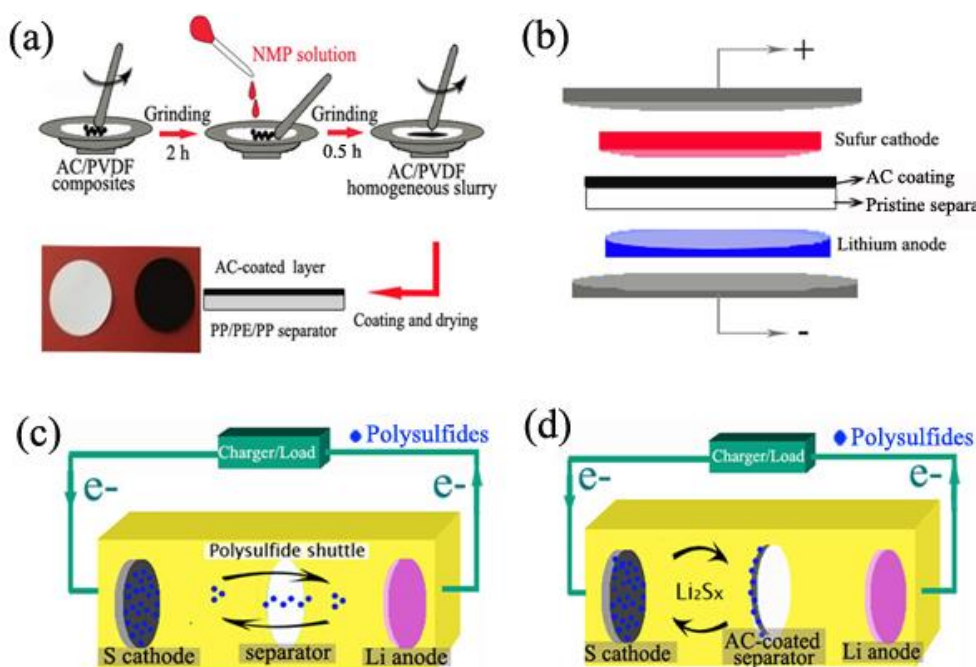


**Figure 1.** (a) Schematic of the AC- $X$  separator preparation. (b) Configuration of a Li-S cell with an AC- $X$  separator. (c) Polysulfide diffusion in Li-S cells with routine separator and (d) inhibition of polysulfide-diffusion in Li-S cells with an AC- $X$  separator.

## 2.3. Materials characterization

The morphology of the AC-coated separators was characterized using a field-emission scanning electron microscopy (FESEM, SEM HITACHIS-4800) with an energy dispersive spectrometer (EDS). Specific surface areas were calculated by the multipoint Brunauer–Emmett–Teller (BET) method at a

relative pressure  $p \cdot p_0^{-1} = 0.05\text{--}0.2$  with Micromeritics ASAP 2020, whereas the total pore was determined at a relative pressure at  $p \cdot p_0^{-1} = 0.97$ . The pore size distribution of mesopores and micropores were measured by Barrett–Joyner–Halenda model and Horvath–Kawazoe model, respectively.

#### 2.4. Battery preparation

The sulfur cathode was prepared by casting a slurry containing 70 wt.% active material, 20 wt.% acetylene black, and 10 wt.% PVDF binder in NMP on the aluminum foil, followed by drying in a vacuum oven at 60 °C for 12 h before cut. All the electrochemical tests for the sulfur cathode were carried out by using CR-2025-type button cells, which were assembled in an argon-filled glove box using AC-X separators/pristine separators and Li metal as the counter electrode. The electrolyte used in this study was 1 M Li TFSI/DME+DOL (1:1, v/v) containing LiNO<sub>3</sub> (1 wt.%). The battery configuration of a Li–S cell with the AC-X separator is displayed in Fig. 1b. Furthermore, the AC-X coating side faces the sulfur cathode.

#### 2.5. Electrochemical measurement

The cells were charged and discharged at different current densities in the voltage range 1.5–2.8 V using the LAND test instrument at a 25 °C constant temperature. The cyclic voltammetry (CV) and electrochemical impedance spectroscopy (EIS) measurements were conducted on a CHI750E electrochemical workstation with a 1.5–3.0 V scanning window and a 0.01 mV s<sup>-1</sup> scanning rate. In EIS tests, the frequency range varied from 0.01 Hz to 100 kHz with an AC signal amplitude of 5 mV.

### 3. RESULTS AND DISCUSSION

#### 3.1. Characterization of routine/AC-coated separator

Figure 1c illustrates the polysulfide diffusion in Li–S cells with routine separator, but in Fig. 1d, the AC-X coating facing the sulfur cathode can function as a physical barrier to block the lithium polysulfides during cycling. In addition, this AC-X with good electrical conductivity offers affluent electron pathways for the insulating sulfur to accelerate fast electron transport[36].

The physical property of AC was characterized by nitrogen physisorption measurements. As shown in Fig. 2, the nitrogen adsorbed at very low pressure ( $p \cdot p_0^{-1} < 0.1$ ) and the well-pronounced hysteresis loop at a high-pressure region ( $p \cdot p_0^{-1} > 0.6$ ) expresses the presence of micropores and mesopores, respectively. The specific surface areas determined by the BET method and the total pore volumes are calculated to be 1386 m<sup>2</sup> g<sup>-1</sup> and 0.21 cm<sup>3</sup> g<sup>-1</sup>, respectively. The pore size distribution is shown in Fig. 2b, which reveals the presence of micropores and mesopores with diameters of 0.5 and 12.8 nm, respectively. In line with the results, we concluded that the AC-X possesses high specific

surface area and dual porosity structure, which are beneficial for inhibiting shuttle effect of polysulfides intermediates and cushioning the volume expansion of the confined sulfur species.

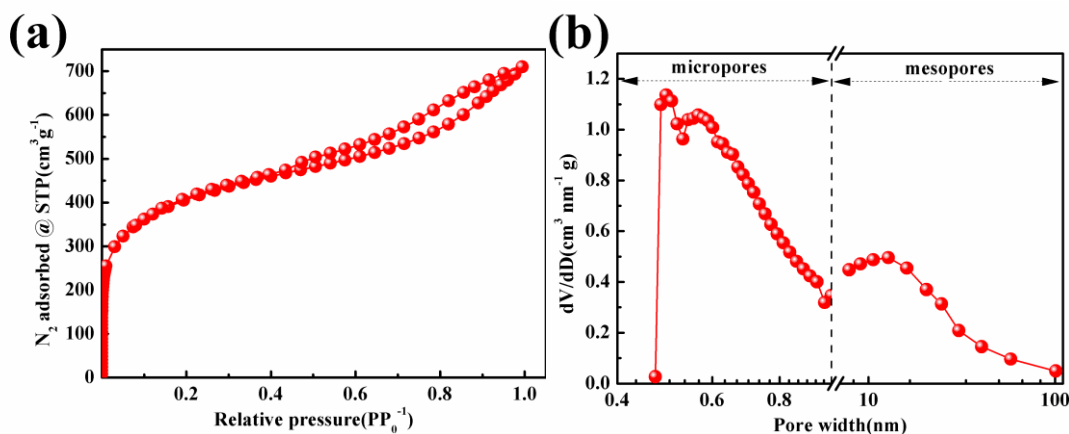


**Figure 2** (a) Nitrogen physisorption isotherms and (b) pore size distributions of AC.

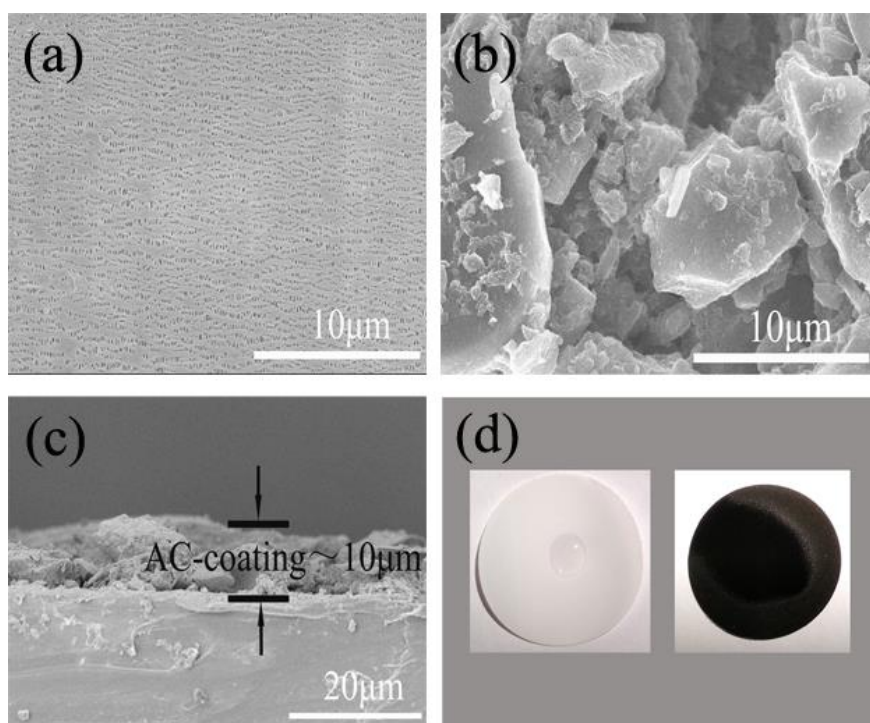


**Figure 3.** SEM images of (a) routine Celgard separator (surface); (b) AC-9 Celgard separator (surface); (c) AC-9 Celgard separator (cross-section). (d) Photographs of the electrolyte on a routine separator and a AC-9 separator.

The morphologies of the routine separator and the AC-9 separator are presented in Fig. 3 (a, b, c). From the images, we can see that the original separator (Fig. 3a) has a smooth surface and highly regular nanoporous structure with abundant slit pores of around 100 nm. Whereas the AC-9 separator (Fig. 3b) consisting of AC particles with different sizes, interconnected by PVDF binder. Meanwhile,

as shown in the picture, AC-9 possesses numerous interconnected voids, which can be filled with liquid electrolyte and provide attachment points for polysulfide species, thus inhibiting the shuttle effect. The cross-section image of the AC-coated separator is presented in Fig. 3c, as one can see that the AC-9 layer adheres well to the surface of original separator and is nearly 10  $\mu\text{m}$  thick.

Figure 3d depicts that the wetted area of AC-9 separator is much larger than the original separator; this result means that the surface hydrophilicity of the separator increased after coating with thin AC layer. The enhanced diffusion ability is affinitive with the restriction of polysulfides and promotes better utilization of active material that consequently improves the performance of Li-S cells.

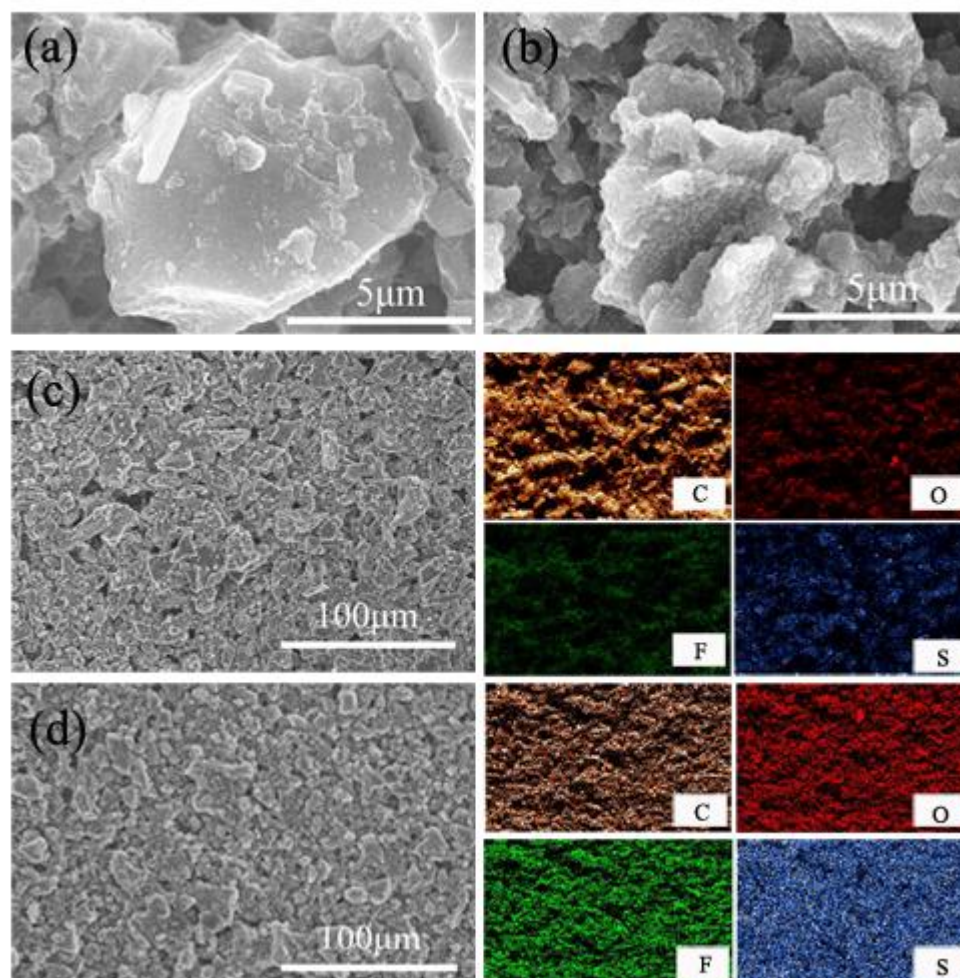


**Figure 4.** High-magnification SEM images of the AC-9 separator (a) before cycling and (b) after 200 cycles at 0.2C. Low-magnification SEM images and elemental mapping of the AC-9 separator (c) before and (d) after 200 cycles at 0.2C.

The comparison charts of the AC-9 separator before and after 200 cycles at 0.2 C are shown in Fig. 4. We can clearly observe the relatively smooth surface of AC particles before cycling (Fig. 4a), whereas the surface becomes rough with innumerable scaly lumps after cycling (Fig. 4b), which means abundant polysulfides were caught and uniformly attached on the surface of AC particles. The SEM image and the corresponding EDS elemental mapping further supported these conclusions. As shown

in Fig. 4c, a small amount of unevenly distributed sulfur was detected, which may be due to the impurities in active carbon. But the elemental S signal is uniformly distributed in the carbon matrix (Fig. 4d) after cycling. Also, elemental oxygen and fluorine are recognizable in AC coating attributing to the outstanding interception ability and excellent electrolyte infiltration of the AC-9 separator.

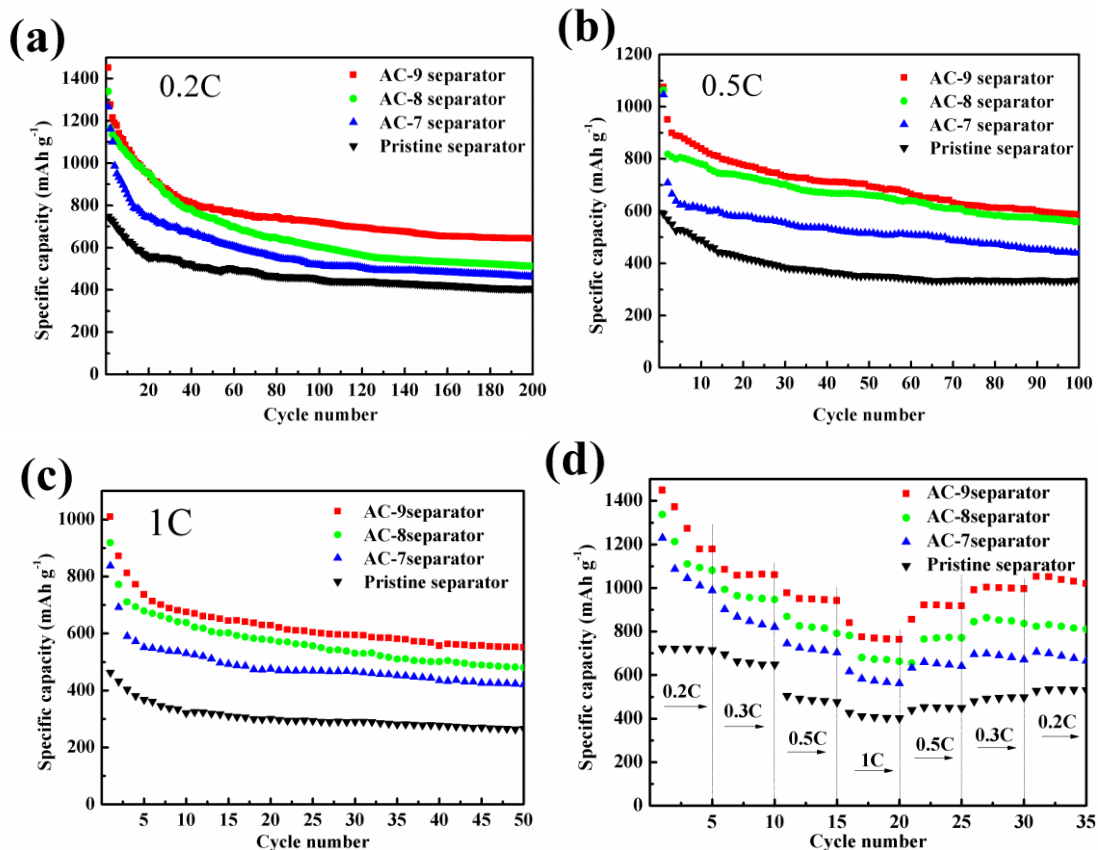
### 3.2. Electrochemical performance of batteries with AC-X separator

To confirm what mass ratio of AC/PVDF-decorated separator can make Li-S cells to possess the best electrochemical performance, cycle performance of the Li-S cells with original separator and AC-X separator at different discharge current densities were measured. As demonstrated in Fig. 5a, the initial discharge capacity of AC-X ( $X = 7, 8, 9$ ) at 0.2 C reach 1267, 1339, and 1452 mAh g<sup>-1</sup>, respectively. After 200 cycles, the reversible discharge capacities of the cells maintain 461, 511, and 643 mAh g<sup>-1</sup>, respectively. In contrast, the cells with pristine separators exhibit poor cycle performance, which implies that the cycle capability of Li-S cells is significantly improved with the increase of AC content. In particular, the AC-9 separator possesses the best cyclic stability, because the AC:PVDF = 9:1 can not only bring out a stable structure for long-term cycling but also keep a high surface area to adsorb a great deal of reaction intermediates, thus largely improves the utilization of active substance. Therefore, the cell with AC-9 separator displays a high initial capacity of 1075 mAh g<sup>-1</sup> at 0.5 C and excellent capacity retention of 586 mAh g<sup>-1</sup> after 100 cycles as shown in Fig. 5b. Furthermore as Fig. 5c depicts, even at a higher rate of 1 C, AC-9 separator battery still shows the best cycle stability.

To better study the electrochemical performance of the cells with AC-X separator, rate performance is demonstrated in Fig. 5d. The rate capability of the Li-S cells with pristine separator and AC-X separator is evaluated by increasing the discharge-charge current density stepwise from 0.2 C to 1 C every five cycles. In Fig. 5d, the initial discharge capacity of the cell with AC-9 separator is as high as 1448 mAh g<sup>-1</sup> (corresponding to 86% utilization of sulfur), and after the original decay stage, the capacity becomes stable when the C-rate increases. The capacity of cell with AC-9 separator decreases slowly from the reversible capacity of 1178 mAh g<sup>-1</sup> at 0.2 C to 1060, 941, and 763 mAh g<sup>-1</sup> at 0.3, 0.5, and 1 C, respectively. Importantly, a satisfactory capacity of 1052 mAh g<sup>-1</sup> (73% of the initial reversible capacity) can be obtained when the current rate was reduced back to 0.2 C, which is obviously larger than the cells with AC-X ( $X = 7, 8$ ) separator and pristine separator, especially at high C-rate; this result demonstrates the effective limitation of polysulfides between the cathode and the AC-9 separator. As listed in Table 1, the initial discharge capacity of separators with single carbon material or metallic oxide is generally low, and after compounding with other materials or doping N/S element, the cycling performance of Li-S cells can be effectively improved. However, these modifications will increase the complexity and cost of the preparation process. Compared the cycling performance of AC-9 separator with the others, we finds that AC-9 coating possess the highest initial discharge capacity and good cycling ability, which demonstrates the excellent electrochemical performance.

**Table 1.** Cycling performance of separators with different coating materials

Coating material	Reference	Current density	Cycling performance/ mAh·g <sup>-1</sup>
AB	[37]	0.05C	1140(before cycling)
CNT	[40]	0.2C	1100(before cycling) 760(150 cycles)
KB	[50]	0.2C	1120(before cycling)
Super P / IPA	[36]	0.2C	1389(before cycling) 828(200 cycles)
CNT / IPA	[42]	0.2C	1324(before cycling) 881(150 cycles)
KB / Super P	[43]	0.1C	1318(before cycling)
N-mesoporous carbon	[44]	0.2C	1364(before cycling) 1040(100 cycles)
N、S-mesoporous carbon	[46]	0.2C	1267 (before cycling) 889(100 cycles)
Al <sub>2</sub> O <sub>3</sub>	[48]	0.2C	967(before cycling) 593(50 cycles)
Al <sub>2</sub> O <sub>3</sub> +Graphene	[49]	0.2C	1067(before cycling) 804 (100 cycles)
M <sub>n</sub> O+KB	[50]	0.2C	1200 (before cycling)
RuO <sub>2</sub> -MPC	[51]	0.2C	859(90 cycles)
AC-9	This work	0.2C	1452(before cycling) 643(200 cycles)
AC-8	This work	0.2C	1339(before cycling) 511(200 cycles)
AC-7	This work	0.2C	1267(before cycling) 461(200 cycles)



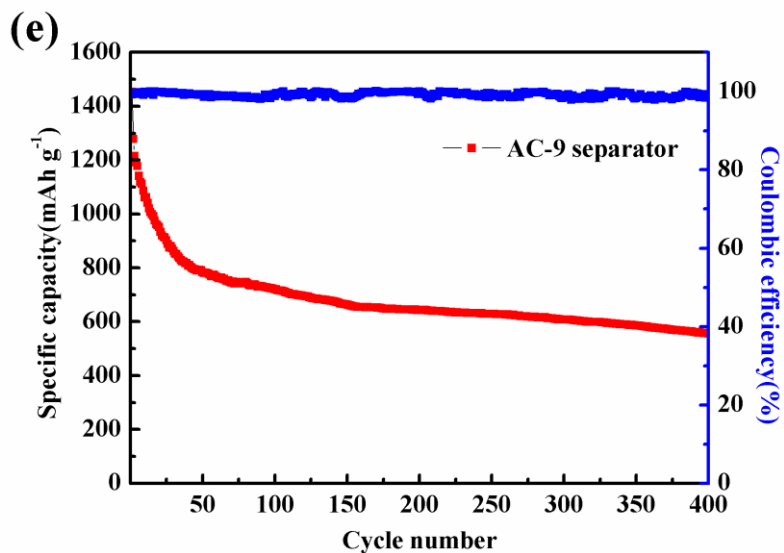


**Figure 5.** Cycle performance of Li-S cells with pristine separator and AC- $X$  ( $X=7, 8, 9$ ) separator at (a) 0.2C, (b) 0.5C, (c) 1C. (d) Rate performance of Li-S cells with pristine separator and AC- $X$  ( $X=7, 8, 9$ ) separator. (e) Long-term cycling performance and Coulombic efficiency of the cell with an AC-9 separator at 0.2C.

The long-term cycling performance and coulombic efficiency of the cell with AC-9 separator was tested at a rate of 0.2 C for 400 cycles as revealed in Fig. 5e. The Li-S cell exhibits good cycle stability, achieving  $555 \text{ mAh g}^{-1}$ , good coulombic efficiency of 98%, and low degradation rate of 0.15% after 400 cycles; these results indicate a superior cycling performance of the Li-S cell that can attribute to the AC-9 coating act as an upper current collector ensures fast electron conduction and ion transport and restrict the diffusion of polysulfides with its dual porosity structure.

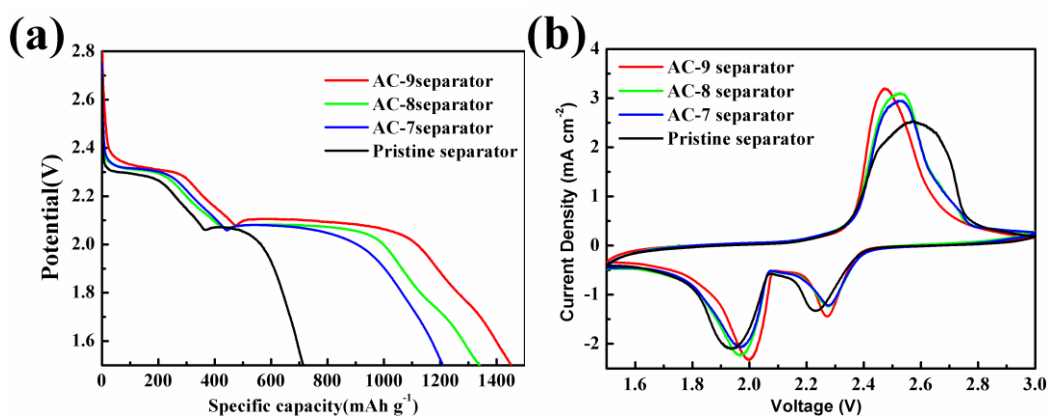


**Figure 6.** (a) Initial discharge profiles of Li-S cells with a pristine separator and an AC- $X$  ( $X=7, 8, 9$ ) separator at 0.2C. (b) Cyclic voltammogram curves of Li-S cells with a pristine separator and an AC- $X$  ( $X=7, 8, 9$ ) separator at a scanning rate of  $0.1 \text{ mV s}^{-1}$ .

The initial discharge profiles of Li-S cells with pristine separator and AC- $X$  separator at 0.2 C are shown in Fig. 6a, this result exhibits two discharge plateaus at around 2.3 and 2.0 V. The upper discharge plateau represents the transformation of sulfur into long-chain polysulfides  $\text{Li}_2\text{S}_x$  ( $4 \leq x \leq 8$ ),

and the lower discharge plateau represents the conversion of the semi-solid phase  $\text{Li}_2\text{S}_4$  to solid phase low-order  $\text{Li}_2\text{S}_2/\text{Li}_2\text{S}$ [53]. In comparison with the Li–S cell with pristine separator, the discharge plateau of AC-X cells is obviously higher, probably due to the improved conductivity and reduced impedance. The length of discharge plateau of AC-9 cell is the longest, which indicates that sulfur can be fully react to form  $\text{Li}_2\text{S}_2/\text{Li}_2\text{S}$ , thus enhances the utilization of active material.

Fig. 6b shows the CV of the cells with pristine separator and AC-X separator for the first cycle within a cutoff voltage window of 1.5–2.8 V at a scan rate of  $0.1 \text{ mV s}^{-1}$ . Two pairs of reduction peaks at around 2.3 and 2.0 V, which are consistent with the discharge profiles, and one oxidation peak at around 2.5V are features of Li–S cells. Importantly, with the increase content of AC, the voltage corresponding to the reduction peaks increases and oxidation peak reduces, respectively, owing to the poor conductivity of PVDF, which leads to the polarization in batteries. Therefore, the AC-9 coated separator can effectively improve the electrochemical performance of Li–S batteries.

To demonstrate the improved conductivity of AC-X-coated separator, EIS of the four samples were tested with frequency from 0.01 Hz to 100 KHz. Moreover, Z-view Software was used to fit an equivalent circuit (Fig. 7, inset). In the equivalent circuit,  $R_1$  denotes the resistance of the electrolyte,  $R_2$  is the charge transfer resistance,  $\text{CPE}_1$  represents the constant-phase elements, and  $W_1$  is the Warburg diffusion impedance[54]. For the cells before the first cycle, as shown in Fig. 7a, the impedance plots are composed of a semicircle at high frequency and medium frequency, corresponding to the charge transfer resistance, and an inclined line at low frequency, which is in accordance with Warburg impedance. Moreover, the intercept at high frequency represents the ohmic resistance[34]. According to the equivalent circuit fitting, the charge transfer resistance of all cells decrease after cycling, which is due to a chemical activation process of the dissolution and redistribution of the active materials[55]. In addition, the resistance of the AC-9 cell is the lowest either before or after 100 cycles at 0.3 C. Due to the superior electrical conductivity and the physical adsorption capacity of the coating material, active substance can be fully used, thus, the performance of Li–S cells is greatly improved.

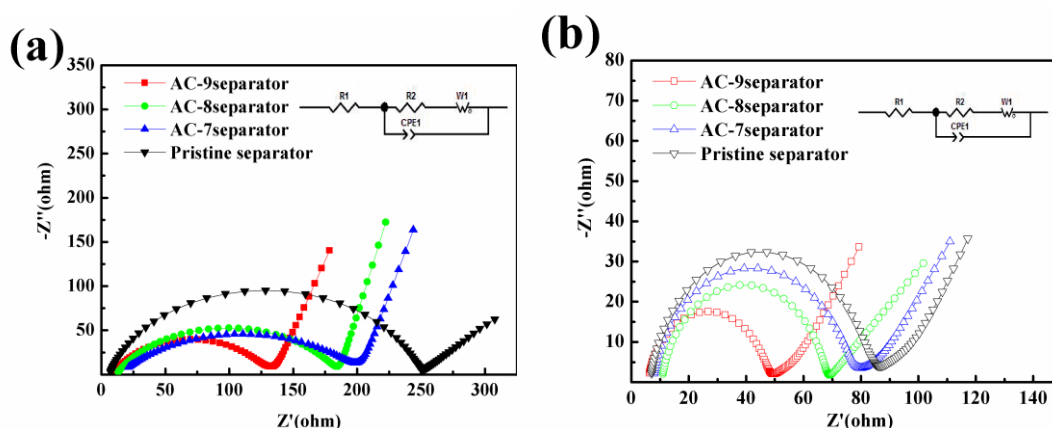


**Figure 7.** Electrochemical impedance spectra of the cells with a pristine separator and an AC-X (X=7, 8, 9) separator (a) before and (b) after the 100th cycle at 0.3C.

#### 4. CONCLUSIONS

In summary, AC- $X$  ( $X = 7, 8, 9$ ) were prepared and used as separator coating of Li-S cells for the first time. This coating is facile, low-cost and significantly improved the performance of the Li-S batteries. With the AC-9 separator, the Li-S cells possess a high initial discharge capacity of 1452 mAh g<sup>-1</sup> and can maintain a discharge capacity of 555 mAh g<sup>-1</sup> after 400 cycles at 0.2C, which is the best among the three composites. Moreover, the cells exhibit the longest discharge platform and the lowest impedance. The excellent results prove that the AC-9 coating possesses the most stable structure when it is guaranteed to contain as much AC as possible. In addition, the good conductivity and superior physical adsorption ability of AC-9 can remarkably improve the electron ion conductivity of Li-S cells and the utilization of sulfur. Compared with other coating materials, the preparation process of AC- $X$  ( $X = 7, 8, 9$ ) coating is simpler and the raw materials are easier to obtain, thus increasing the possibility of the practical application and offers a promising strategy to improve Li-S batteries.

#### ACKNOWLEDGEMENTS

This work was supported by the National Natural Science Foundation of China (Grant No. 11364011) and the Guangxi Natural Science Foundation (Grant No. 2015GXNSFAA139004).

#### References

1. S. Aziz, J. Zhao, C. Cain and Y. Wang, *J Mater Sci Technol*, 30 (2014) 427-433.
2. Y.X. Chen, L.H. He, P.J. Shang, Q.L. Tang, Z.Q. Liu, H.B. Liu and L.P. Zhou, *J Mater Sci Technol*, 27 (2011) 41-45.
3. M. Wang, A.V. Le, Y. Shi, D.J. Noelle, H. Yoon, M. Zhang, Y.S. Meng and Y. Qiao, *J Mater Sci Technol*, 32 (2016) 1117-1121.
4. W.C. Du, Y.X. Yin, X.X. Zeng, J.L. Shi, S.F. Zhang, L.J. Wan and Y.G. Guo, *ACS Appl Mater Interfaces*, 8 (2016) 3584-3590.
5. C. Xu, H. Zhou, C. Fu, Y. Huang, L. Chen, L. Yang and Y. Kuang, *Electrochim Acta*, 232 (2017) 156-163.
6. Y. Xie, Z. Meng, T. Cai and W.Q. Han, *ACS Appl Mater Interfaces*, 7 (2015) 25202-25210.
7. S. Urbonaite, T. Poux and P. Novák, *Advanced Energy Materials*, 5 (2015) 1500118.
8. L. Ji, M. Rao, H. Zheng, L. Zhang, Y. Li, W. Duan, J. Guo, E.J. Cairns and Y. Zhang, *J Am Chem Soc*, 133 (2011) 18522-18525.
9. D.-W. Wang, Q. Zeng, G. Zhou, L. Yin, F. Li, H.-M. Cheng, I.R. Gentle and G.Q.M. Lu, *Journal of Materials Chemistry A*, 1 (2013) 9382.
10. S. Xin, L. Gu, N.H. Zhao, Y.X. Yin, L.J. Zhou, Y.G. Guo and L.J. Wan, *J Am Chem Soc*, 134 (2012) 18510-18513.
11. G. Xu, B. Ding, P. Nie, L. Shen, H. Dou and X. Zhang, *ACS Appl Mater Interfaces*, 6 (2014) 194-199.
12. S. Xiong, K. Xie, Y. Diao and X. Hong, *Electrochim Acta*, 83 (2012) 78-86.
13. Z. Zhang, G. Wang, Y. Lai, J. Li, Z. Zhang and W. Chen, *J Power Sources*, 300 (2015) 157-163.
14. J. Akridge, *Solid State Ionics*, 175 (2004) 243-245.
15. Y. Deng, H. Xu, Z. Bai, B. Huang, J. Su and G. Chen, *J Power Sources*, 300 (2015) 386-394.
16. P. Wei, M.Q. Fan, H.C. Chen, X.R. Yang, H.M. Wu, J. Chen, T. Li, L.W. Zeng, C.M. Li, Q.J. Ju, D.

- Chen, G.L. Tian and C.J. Lv, *Renew Energ*, 86 (2016) 148-153.
17. H.H. Nersisyan, S.H. Joo, B.U. Yoo, D.Y. Kim, T.H. Lee, J.-Y. Eom, C. Kim, K.H. Lee and J.-H. Lee, *Carbon*, 103 (2016) 255-262.
  18. H. Li, L. Sun and G. Wang, *ACS Appl Mater Interfaces*, 8 (2016) 6061-6071.
  19. S. Rehman, S. Guo and Y. Hou, *Adv Mater*, 28 (2016) 3167-3172.
  20. J. Zhang, H. Ye, Y. Yin and Y. Guo, *J Energy Chem*, 23 (2014) 308-314.
  21. J. Lee, T. Hwang, Y. Lee, J.K. Lee and W. Choi, *Mater Lett*, 158 (2015) 132-135.
  22. H. Tang, S. Yao, M. Jing, X. Wu, J. Hou, X. Qian, D. Rao, X. Shen, X. Xi and K. Xiao, *J Alloy Compd*, 650 (2015) 351-356.
  23. Z. Gong, Q. Wu, F. Wang, X. Li, X. Fan, H. Yang and Z. Luo, *RSC Adv.*, 6 (2016) 37443-37451.
  24. W. Deng, A. Hu, X. Chen, S. Zhang, Q. Tang, Z. Liu, B. Fan and K. Xiao, *J Power Sources*, 322 (2016) 138-146.
  25. D.H. Wang, X.H. Xia, D. Xie, X.Q. Niu, X. Ge, C.D. Gu, X.L. Wang and J.P. Tu, *J Power Sources*, 299 (2015) 293-300.
  26. W. Yang, W. Yang, J. Feng, Z. Ma and G. Shao, *Electrochim Acta*, 210 (2016) 71-78.
  27. Z. Jin, K. Xie, X. Hong and Z. Hu, *J Power Sources*, 242 (2013) 478-485.
  28. J.-Q. Huang, Z.-L. Xu, S. Abouali, M. Akbari Garakani and J.-K. Kim, *Carbon*, 99 (2016) 624-632.
  29. Y. Yang, W. Sun, J. Zhang, X. Yue, Z. Wang and K. Sun, *Electrochim Acta*, 209 (2016) 691-699.
  30. X. Wang, Z. Wang and L. Chen, *J Power Sources*, 242 (2013) 65-69.
  31. C. Zu, Y.S. Su, Y. Fu and A. Manthiram, *Phys Chem Chem Phys*, 15 (2013) 2291-2297.
  32. Y.S. Su and A. Manthiram, *Nat Commun*, 3 (2012) 1166.
  33. L.-B. Xing, K. Xi, Q. Li, Z. Su, C. Lai, X. Zhao and R.V. Kumar, *J Power Sources*, 303 (2016) 22-28.
  34. Z. Zhang, Y. Lai, Z. Zhang and J. Li, *Solid State Ionics*, 278 (2015) 166-171.
  35. H. Wei, J. Ma, B. Li, Y. Zuo and D. Xia, *ACS Appl Mater Interfaces*, 6 (2014) 20276-20281.
  36. S.-H. Chung and A. Manthiram, *Adv Funct Mater*, 24 (2014) 5299-5306.
  37. N. Liu, B. Huang, W. Wang, H. Shao, C. Li, H. Zhang, A. Wang, K. Yuan and Y. Huang, *ACS Appl Mater Interfaces*, 8 (2016) 16101-16107.
  38. G. Zhou, L. Li, D.W. Wang, X.Y. Shan, S. Pei, F. Li and H.M. Cheng, *Adv Mater*, 27 (2015) 641-647.
  39. H.J. Peng, D.W. Wang, J.Q. Huang, X.B. Cheng, Z. Yuan, F. Wei and Q. Zhang, *Adv Sci (Weinh)*, 3 (2016) 1500268.
  40. H. Yao, K. Yan, W. Li, G. Zheng, D. Kong, Z.W. Seh, V.K. Narasimhan, Z. Liang and Y. Cui, *Energy Environ. Sci.*, 7 (2014) 3381-3390.
  41. G. Wang, Y. Lai, Z. Zhang, J. Li and Z. Zhang, *J. Mater. Chem. A*, 3 (2015) 7139-7144.
  42. S.H. Chung and A. Manthiram, *J Phys Chem Lett*, 5 (2014) 1978-1983.
  43. D. Zhao, X. Qian, L. Jin, X. Yang, S. Wang, X. Shen, S. Yao, D. Rao, Y. Zhou and X. Xi, *RSC Adv.*, 6 (2016) 13680-13685.
  44. J. Balach, T. Jaumann, M. Klose, S. Oswald, J. Eckert and L. Giebeler, *J Power Sources*, 303 (2016) 317-324.
  45. X. Zhou, Q. Liao, J. Tang, T. Bai, F. Chen and J. Yang, *J Electroanal Chem*, 768 (2016) 55-61.
  46. J. Balach, H.K. Singh, S. Gomoll, T. Jaumann, M. Klose, S. Oswald, M. Richter, J. Eckert and L. Giebeler, *ACS Appl Mater Interfaces*, 8 (2016) 14586-14595.
  47. Z. Li, Q. Jiang, Z. Ma, Q. Liu, Z. Wu and S. Wang, *RSC Adv.*, 5 (2015) 79473-79478.
  48. Z. Zhang, Y. Lai, Z. Zhang, K. Zhang and J. Li, *Electrochim Acta*, 129 (2014) 55-61.
  49. R. Song, R. Fang, L. Wen, Y. Shi, S. Wang and F. Li, *J Power Sources*, 301 (2016) 179-186.
  50. X. Qian, L. Jin, D. Zhao, X. Yang, S. Wang, X. Shen, D. Rao, S. Yao, Y. Zhou and X. Xi, *Electrochim Acta*, 192 (2016) 346-356.
  51. J. Balach, T. Jaumann, S. Muhlenhoff, J. Eckert and L. Giebeler, *Chem Commun (Camb)*, 52 (2016) 8134-8137.

52. X. Jianrong, Z. Hang, J. Aihua, W. Hongzhe and L. Yanwei, *Ionics*, 21 (2014) 1241-1246.
53. J. Zhu, Y. Ge, D. Kim, Y. Lu, C. Chen, M. Jiang and X. Zhang, *Nano Energy*, 20 (2016) 176-184.
54. Y. Hou, J. Xiao, Y. Guo, M. Qi, A. Jiang and Y. Li, *J Mater Sci-Mater El*, (2017).
55. J. Xie, J. Yang, X. Zhou, Y. Zou, J. Tang, S. Wang and F. Chen, *J Power Sources*, 253 (2014) 55-63

© 2017 The Authors. Published by ESG ([www.electrochemsci.org](http://www.electrochemsci.org)). This article is an open access article distributed under the terms and conditions of the Creative Commons Attribution license (<http://creativecommons.org/licenses/by/4.0/>).